Pure appl. geophys. 158 (2001) 1737–1761
0033–4553/01/101737–25 $ 1.50 + 0.20/0

Pure and Applied Geophysics

Coda Q_c Attenuation and Source Parameter Analysis in Friuli (NE Italy) and its Vicinity

D. D. Singh,[1] Aladino Govoni[2] and Pier Luigi Bragato[2]

Abstract — The digital data acquired by 16 short-period seismic stations of the Friuli-Venezia-Giulia seismic network for 56 earthquakes of magnitude 2.3–4.7 which occurred in and near NE Italy have been used to estimate the coda attenuation Q_c and seismic source parameters. The entire area under study has been divided into five smaller regions, following a criterion of homogeneity in the geological characteristics and the constrains imposed by the distribution of available events. Standard IASPEI routines for coda Q_c determination have been used for the analysis of attenuation in the different regions showing a marked anomaly in the values measured across the NE border between Friuli and Austria for Q_0 value. A large variation exists in the coda attenuation Q_c for different regions, indicating the presence of great heterogeneities in the crust and upper mantle of the region. The mean value of $Q_c(f)$ increases from 154–203 at 1.5 Hz to 1947–2907 at 48 Hz frequency band with large standard deviation estimates.

Using the same earthquake data, the seismic-moment, M_0, source radius, r and stress-drop, $\Delta\sigma$ for 54 earthquakes have been estimated from *P*- and *S*-wave spectra using the Brune's seismic source model. The earthquakes with higher stress-drop (greater than 1 Kbar) occur at depths ranging from 8 to 14 km.

Key words: Coda wave attenuation, seismic source parameters, Friuli.

Introduction

Attenuation studies are useful to determine the source mechanism, to estimate earthquake magnitude, to find the range of detection capability of seismic signals and to detect the presence of anomalous zones such as partial melting or magma chambers in the crust and upper mantle. The evaluation of seismic attenuation parameters using local earthquakes has recently become routine work due to the simple method for estimating the quality factor Q of coda waves or coda attenuation Q_c, based on the single-scattering model developed by Aki and Chouet (1975) and Sato (1977). Subsequently numerous studies have been made using the coda waves from local earthquakes world wide (e.g., Aki, 1980; Roecker *et al.*, 1982; Pulli, 1984; Phillips, 1985; Del Pezzo and Scarcella, 1986; Havskov *et al.*, 1989;

[1] National Geophysical Research Institute, Hyderabad-500007, India.
[2] Osservatorio Geofisico Sperimentale, DPT. Centro Riche Sismologiche, C.P. 1 Cussignacco (Udine), Italy. E-mail: aladino/bragato@sparc5.crs.ogs.trieste.it

KVAMME and HAVSKOV, 1989; IBANEZ, 1990; PUJADES *et al.*, 1990; CANAS *et al.*, 1991). Studies have been made in Friuli, a region of NE Italy, using strong motion records and seismograms of local earthquakes to estimate the attenuation parameter Q_c (CONSOLE and ROVELLI, 1981; ROVELLI, 1982, 1983). These studies have been aimed to determine a mean Q_c value of the region which is seismically active. In the present study we estimate the 2-D distribution of coda attenuation Q_0 for NE Italy and its nearby regions, using several hundred of the seismic wave propagation paths.

The entire area has been subdivided into five smaller regions A to E (also shown in Fig. 1) in order to separate different geological characteristics using the seismotectonic analysis of SLEJKO *et al.* (1989). The subdivision of the regions (A to E) has also been constrained by the availability of seismic events. The distribution of epicentres covers most uniformly throughout the regions A, B, and C. In region E epicentres are quite aligned along the WE direction following the base of the Alps mountain chain up to the beginning of Slovenia, while region D is less covered by

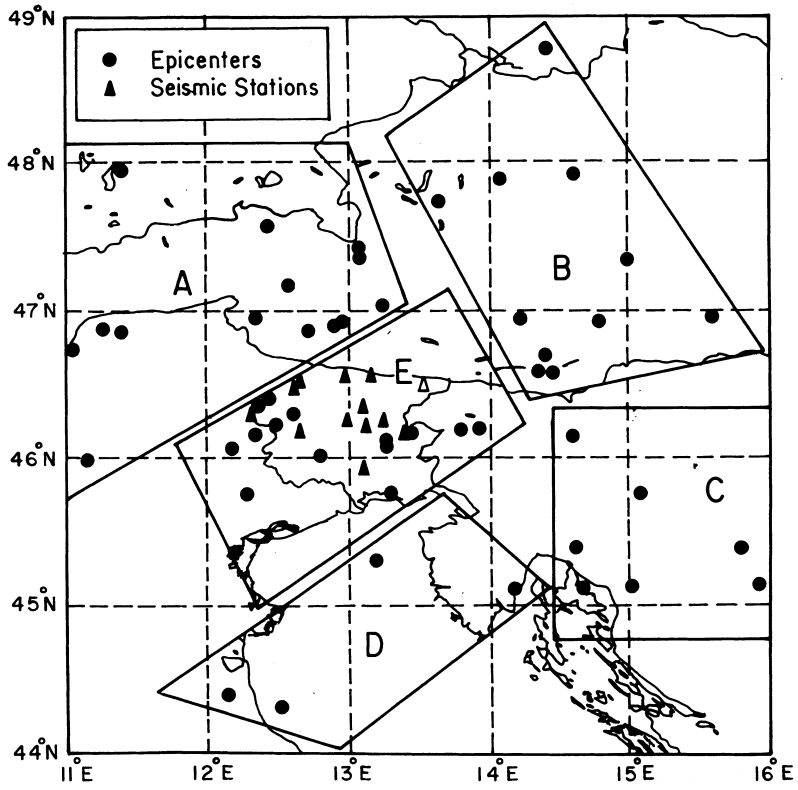

Figure 1
The epicentre of earthquakes (circles) and the location of seismic stations (triangles) are shown with the borders of five regions marked by letters A, B, C, D and E.

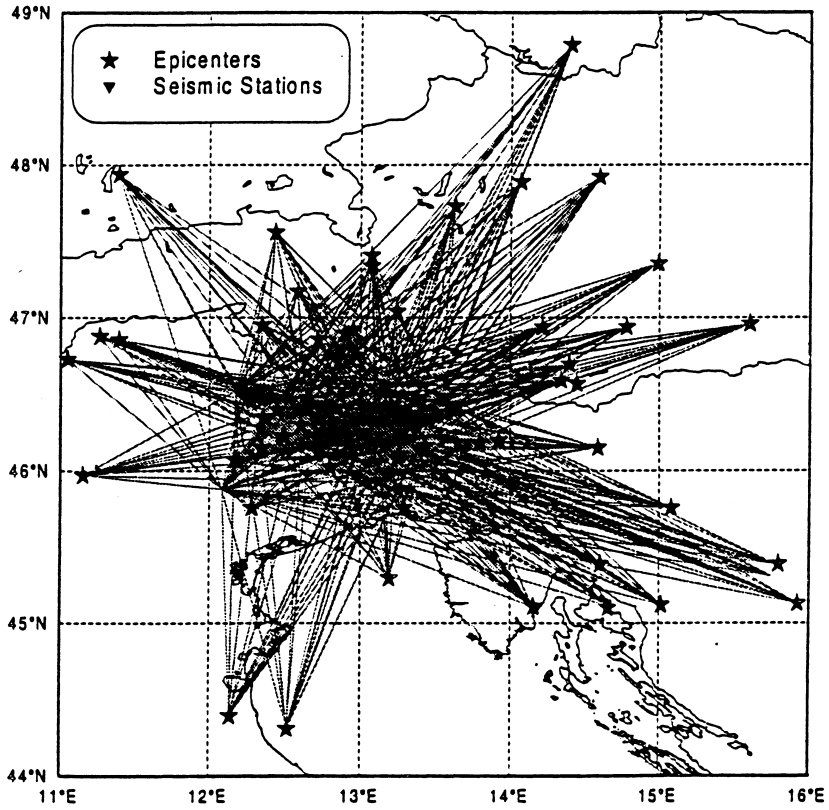

Figure 2
Propagation paths used for Q_c estimation.

seismic events. In Figure 2, propagation paths joining epicentres and stations are represented to indicate the crust volume crossed by the earthquake waves selected in this data set.

The seismic source parameters such as stress-drop and source radius are useful for understanding the tectonic stress variation in different seismotectonic environments. The stress-drop, apparent stress and source radius for the main Friuli earthquake of May 6, 1976 and its aftershock sequences have been estimated by CIPAR (1980), DE NATALE *et al.* (1987), COCCO and ROVELLI (1989). Recently, differences in the short-period spectral amplitudes due to the variation of the stress-drop have been found using the data of various tectonic regimes (ZHUO and KANAMORI, 1987), and this finding suggests that the ambient stress environments present in the crust and upper mantle may affect the spectral properties of the ground motion. These investigations have important implications for the seismic risk evaluation studies. We have estimated the stress-drop and source radius for 54 earthquakes mentioned earlier. In the present investigation, the main objective was to

examine the spectral parameters of *P*, *S* and coda waves to study the seismic source parameters such as seismic-moment, source radius and stress-drop of 54 earthquakes in NE Italy and its nearby regions and the 2-D distribution of coda attenuation Q_0 in the region, which will advance understanding of the seismotectonics of the region. The present study may further be useful in the seismic hazard mitigation related research work.

Seismotectonics of the Study Area

The northern sector of the southeastern Alps has been divided into regions A and B. This large area includes the northern part of the Giudicarie system, the Dolomites synclinorium and the Paleocarnic chain. The region is characterized by a very thick crust (≥50 km) with differential uplifting and exhibits a low seismic activity (SLEJKO *et al.*, 1989). Region C includes the external Dinarides and it is characterized by a dextral strike-slip faulting along major faults striking NW-SE. In this region Moho deepens to an elongated NW-SE zone (depth > 40 km) trending parallel to the surface structures, and corresponding to the area of highest earthquake density and crustal thickness is ≥40 km (SLEJKO *et al.*, 1989). There is evidence of crustal thickening and the region is considered to be affected by intracrustal and detachment phenomena. Region D extends over the northern part of the Adriatic Sea and is characterized by normal or thin (≤30 km) crust, which includes the Quaternary southalpine foreland and probably the NW-SE active transcurrent faults. Region E is the Friuli area. The area is located in the eastern part of the southern Alps and consists mainly of sedimentary rock formations of Palaeozoic to Quaternary age. There is a subvertical fault trending East-West and extending throughout the whole region with dextral transcurrent movements and it marks a tectonic contact between Palaeozoic and Mesozoic deposits. The region manifests high neotectonic deformation, a northward deepening of the Moho and a high seismicity that is mainly due to the interaction between the Alpine and Dinaric structures.

Data Analysis

Figure 1 shows the location of earthquake epicentres and seismic stations. All seismic stations used in the analysis are equipped with a Willmore MKIIIA 1 Hz vertical velocity meter, data are transmitted to a Central Earth Data Unit that performs the A/D conversion at 360 Hz and all the necessary preprocessing of the signals.

In the present study we have studied the seismic source parameter of 54 earthquakes and the coda attenuation Q_c over a much larger area compared to earlier studies in different tectonic environments of NE Italy and its environs using the data

of several hundred seismic wave propagation paths. For this purpose we have selected 56 earthquakes with magnitudes ranging from 2.3 to 4.7, covering the entire azimuth range of the Friuli region (Fig. 1; Table 1) spanning 1988–1994. These earthquakes were recorded at the Friuli Venezia Giulia seismic network by 16 short-period seismometers, using a digital acquisition system.

(a) Q Coda

The observed coda attenuation Q_c is thought to be a combination of two different loss mechanisms: (i) due to an intrinsic effect Q_i and (ii) due to a scattering process Q_{sc}. The scattering effect simply redistributes the energy throughout the medium, however if does not remove it from the overfield, and the proportion of scattered energy depends on the ratio between the wavelength and the size of the obstacle. Intrinsic attenuation refers to various mechanisms that convert vibration energy into heat through friction, viscosity and thermal relaxation process (SATO and FELLER, 1998). There are serveral mechanisms of intrinsic attenuation like crack aspect ratio (ratio of width to length of a crack); frictional sliding on dry surfaces of this crack; flow of fluids within nonconnecting pores initiated by elastic waves; fluid movement within cracks; thermally activated processes at grain boundaries (SATO and FELLER, 1998). AKI (1980) has produced a thermo-elasticity model to explain the intrinsic attenuation at lithospheric temperatures.

ROECKER *et al.* (1982), PULLI (1984) and DEL PEZZO *et al.* (1990) have observed an increase of coda Q_c with lapse time (time after the origin time of the earthquake). An increase of coda Q_c with lapse time can be due to several circumstances (WOODGOLD, 1994), such as (i) a nonzero source-receiver distance and a model which does not account for it, (ii) a nonzero source-receiver distance combined with nonisotropic scattering, (iii) use of a two-dimensional (2-D) model whereas a three-dimensional (3-D) model is more appropriate, (iv) use of a single scattering model whereas the multiple scattering model is significant, (v) an increase of Q_c with depth, (vi) an increase of Q_c with distance from source to receiver.

The difference in the coda attenuation for short and long lapse times can be partly explained if we consider that the early coda consists of surface waves and or near-surface reverberations undergoing a relatively rapid decay. As these arrivals are damped out, energy scattered from deeper in the crust may dominate the coda and cause a more gradual decay because of higher intrinsic Q_i at depth (FRANKEL, 1991). Also, in a strongly scattering medium at longer lapse times, most of the energy will be included in the coda and the measured Q_c will be close to Q_i (DAINTY *et al.*, 1987).

The seismograms with best signal-to-noise ratio have been selected and processed for the coda Q_c estimate (VALDES and NOVELO-CASANOVA, 1989). Coda attenuation Q_c values have been estimated at different frequency bands (1.5, 3, 6, 12, 24 and 48 Hz) for each region under study (A, B, C, D and E), using the three methods available in the package.

Table 1

Details of the earthquake parameters used in the study

Sl. No.	Region	Origin time (GMT)	Magnitude	Epicentre		Focal depth (km)
				Latitude (°N)	Longitude (°E)	
01	A	1988:01:02 00:24:41.28	2.9	46.86	11.39	13.0
02	C	1988:01:06 07:47:32.92	2.8	45.39	14.60	13.5
03	B	1988:01:11 02:46:39.17	3.1	47.36	14.98	2.0
04	D	1988:01:19 20:34:55.20	3.4	44.31	12.51	7.0
05	A	1988:02:14 09:41:17.48	3.0	46.73	11.05	9.9
06	D	1988:02:16 23:47:39.20	3.3	44.39	12.14	14.3
07	D	1988:02:19 13:54:14.08	2.8	45.11	14.15	5.6
08	E	1988:02:24 06:16:13.65	2.7	46.29	12.59	7.4
09	E	1988:02:24 15:11:53.46	2.7	46.15	12.34	7.8
10	B	1988:03:06 18:48:46.40	2.5	47.89	14.07	5.0
11	A	1988:03:11 06:14:04.06	2.6	47.56	12.43	3.5
12	E	1988:03:11 21:16:36.91	2.6	46.06	12.19	2.8
13	C	1988:03:14 04:43:17.08	2.6	45.31	15.74	10.0
14	A	1988:03:15 03:30:35.93	2.9	46.92	12.95	12.1
15	B	1988:04:02 10:54:11.82	2.8	46.96	15.60	11.3
16	C	1988:04:05 06:28:02.71	3.2	45.13	15.92	15.8
17	E	1988:04:18 17:28:57.10	2.7	46.07	12.16	10.0
18	E	1988:04:18 18:35:06.03	3.7	46.07	12.17	12.2
19	B	1988:06:10 14:33:54.17	2.5	47.73	13.63	2.7
20	E	1988:08:14 02:56:16.37	2.9	46.16	13.43	12.4
21	A	1988:08:19 01:13:18.82	2.7	47.17	12.58	4.0
22	E	1988:11:06 19:13:18.00	2.6	46.35	12.35	7.3
23	C	1988:12:16 11:35:51.90	4.0	45.76	15.08	12.3

Table 1

Continued

Sl. No.	Region	Origin time (GMT)	Magnitude	Epicentre		Focal depth (km)
				Latitude (°N)	Longitude (°E)	
24	A	1989:07:16 22:10:55.08	2.6	47.40	13.07	2.2
25	A	1989:07:18 19:56:10.7	3.3	47.34	13.07	1.0
26	E	1989:08:22 13:20:19.99	3.1	45.76	12.28	11.4
27	A	1989:09:13 21:54:01.50	4.7	46.88	11.26	9.5
28	C	1989:09:30 18:16:01.48	3.5	45.12	15.01	12.1
29	C	1989:10:24 08:06:00.77	4.5	45.39	15.76	10.6
30	A	1990:01:06 16:36:04.77	3.1	46.89	12.89	13.3
31	E	1990:03:12 12:08:41.74	2.9	46.23	12.48	10.9
32	E	1990:03:27 19:16:06.01	3.0	45.76	13.29	5.0
33	A	1990:05:29 18:53:47.97	3.3	45.97	11.15	12.7
34	B	1990:06:01 20:21:28.57	2.9	48.79	14.39	2.6
35	A	1990:06:28 19:30:09.69	3.4	46.95	12.34	12.4
36	E	1990:07:12 14:52:36.44	3.6	46.22	12.49	10.1
37	A	1990:08:20 13:33:38.73	3.3	47.93	11.39	4.1
38	A	1990:09:17 16:15:33.25	2.5	47.04	13.24	13.8
39	E	1991:06:10 19:18:32.58	2.5	46.19	13.92	10.4
40	C	1991:07:02 01:06:54.24	2.9	45.11	14.67	25.9
41	E	1991:09:27 11:41:25.36	2.9	46.02	12.79	8.1
42	A	1991:10:11 18:43:01.40	3.0	46.85	12.72	6.9
43	C	1992:02:20 21:18:27.68	3.0	46.15	14.58	13.4
44	B	1992:05:24 12:37:59.11	2.5	47.92	14.59	11.8
45	B	1992:08:02 02:41:38.13	3.0	46.95	14.21	16.0
46	D	1992:08:04 07:33:47.97	2.9	45.29	13.19	13.6

Table 1

Continued

Sl. No.	Region	Origin time (GMT)	Magnitude	Epicentre		Focal depth (km)
				Latitude (°N)	Longitude (°E)	
47	E	1992:08:08 07:05:13.55	2.7	46.18	13.79	16.2
48	B	1992:08:25 01:35:18.54	3.2	46.69	14.39	3.8
49	B	1992:09:23 10:52:51.45	3.0	46.94	14.78	12.9
50	E	1992:11:26 10:49:38.35	2.9	46.09	13.25	11.4
51	E	1993:01:12 11:06:59.88	2.6	46.39	12.44	11.7
52	E	1993:07:23 19:34:08.84	3.6	46.11	13.26	10.0
53	B	1993:12:09 09:33:49.64	3.2	46.59	14.33	12.0
54	E	1994:08:18 18:35:25.93	3.1	46.36	13.52	11.8
55	E	1994:08:18 16:40:51.05	2.3	46.27	13.29	12.6
56	E	1994:12:05 21:14:09.09	3.0	46.39	13.66	12.7

In the model of AKI and CHOUET (1975) the coda consists of backscattered *S* waves in a medium with source and receiver in the same location. In this model the scattering is weak enough so that the multiple scattering may be ignored. The model of AKI and CHOUET (1975) is valid for coda waves arriving after twice the *S*-wave travel time. SATO's (1977) model uses a correction term corresponding to the geometrical spreading factor and this model is valid even for coda waves arriving immediately after the *S*-wave arrival. In LEE *et al.* (1986), PHILLIPS and AKI (1986) models, the coda attenuation measurement employs heavy smoothing in the frequency domain, thus the stability is gained, but frequency resolution is diminished. In these models, the coda waves arriving immediately after the *S*-wave arrival or twice the *S*-wave travel time are used.

We have used a sliding time window with the size of 2048 data samples (corresponding to roughly 5.68 sec.) and then advanced through the coda length of 20–110 sec for all the propagation paths in the present study.

Only Q_c values with an error ≤5% have been selected for each processed trace, and among the three results output by QCODA package (VALDES and NOVELO-CASANOVA, 1989) the one with the minimum error has been selected as the appropriate coda Q_c for that propagation path. For each region we obtain several Q_c values,

depending on the number of paths. The mean and standard deviations are estimated for different frequencies, using the data of several path Q_c values. Results are reported in Table 2 and a comparison with those obtained in similar works for other parts of Europe is plotted in Figure 3. Our values are in the same order of magnitude but tend to be high, especially if compared with those found by ROVELLI (1983) for the same area. These values have been fitted to the power law as given below:

$$Q_c(f) = Q_0(f/f_0)^{\eta}.$$

Here Q_0 is the quality factor at a reference frequency (1 Hz) f_0 and η is indicative of the degree of heterogeneity of the crust (AKI, 1981).

Problems arise not only because of the huge standard deviation of the data but also because of high frequency values (an example is presented for region C in Figure 4 to justify the necessity to limit the bandwidth of the fit to 12 Hz). Values of Q_0 and η are listed in Table 3.

Major errors in the estimated values have pointed to the necessity of a considerably numerical analysis to verify this result. A new program has been written, aimed at achieving automatic selection of the traces to be processed with more numerical efficiency.

This program processes the entire coda record, dividing the whole record length of data into several segments of 256 data samples and then processes each segment of 256 data samples separately from the beginning to the end of the coda signal length. Coda $Q_c(f)$ is estimated for each segment of 256 data samples and the entire process is repeated until the coda signal reaches the end position. The coda $Q_c(f)$ values obtained for each segment of data samples are then averaged. In this way the coda $Q_c(f)$ value is independent of coda lapse time and the average value of coda $Q_c(f)$ is estimated for each trace at different frequencies.

This program has control in several parameters affecting the coda determination, among which the more important is the length of the time window (lapse time) used in the coda regression. To lower the processing time and CPU load, that especially with

Table 2

Mean value of coda attenuation Q_c estimates along with standard deviation at different frequency bands for the various regions

f (Hz)	Region A		Region B		Region C		Region D		Region E	
	Q_c	σQ_c	Q_c	σQ_c	Q_c	σQ_c	Q_c	σQ_c	Q_c	σQ_c
1.5	203.4	130.7	154.2	118.2	192.6	94.1	163.9	154.8	162.2	158.0
3.0	551.7	590.9	338.2	204.9	393.7	174.7	304.5	366.2	474.3	512.3
6.0	806.6	442.9	939.0	520.7	978.2	183.7	547.6	565.0	1030.2	485.0
12.0	1452.8	1190.1	2288.2	1582.1	1845.9	847.0	1112.6	1314.7	1854.4	784.6
24.0	1852.4	1295.6	1838.2	1827.0	1994.1	1159.1	1081.7	1152.4	1987.3	1040.0
48.0	2906.7	2862.9	2732.4	1945.6	1946.9	1106.8	2764.4	2564.8	1993.3	965.8

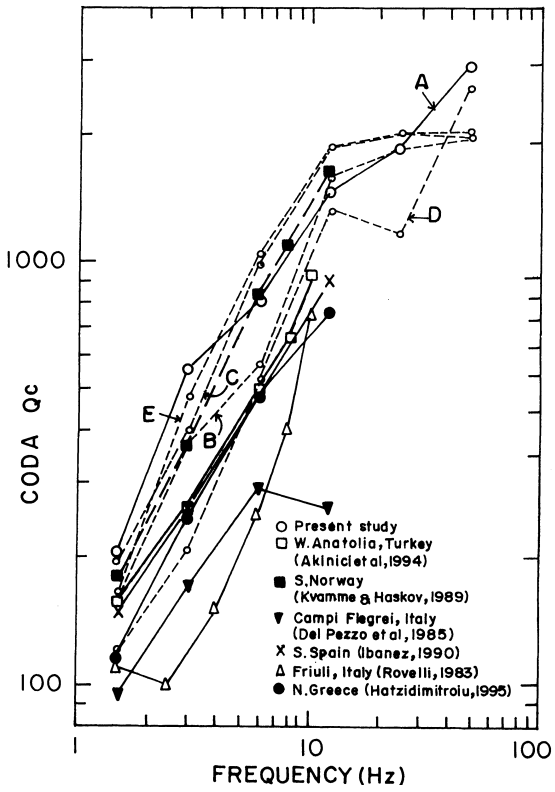

Figure 3
A comparison of the frequency dependence of coda Q_c estimates in the present study with other coda Q_c values in the world.

large data sets are important factors; the traditional time domain band pass filtering has been discarded. The coda amplitude $A(f|t_k)$ has been computed in one pass on a set of half-overlapping time windows centred on t_k, using standard FFT techniques. Due to the high sampling rate used in data acquisition, a good tradeoff between frequency resolution and the stability of the spectral amplitude has been reached. With a time window of $\approx$2.5 s it has been possible to compute the spectrum with a frequency resolution of 1.4 Hz, averaged over 7 overlapping sectors to reduce the spectral variance per data points. The time windows overlap one half of the time length of the signal. The data set has been reprocessed with a higher control for the poor signal-to-noise ratio traces at fixed coda time windows (lapse time), obtaining similar evidence of the anomaly of the values of the B region. All Q_c values have been obtained and then averaged to derive the mean, using the inverse of least-squares fit χ^2 as weight over coda regression performed on the same time window. Stepping the time window τ from 20 s to 80 s, a significant dependence of Q_0 has been verified for all

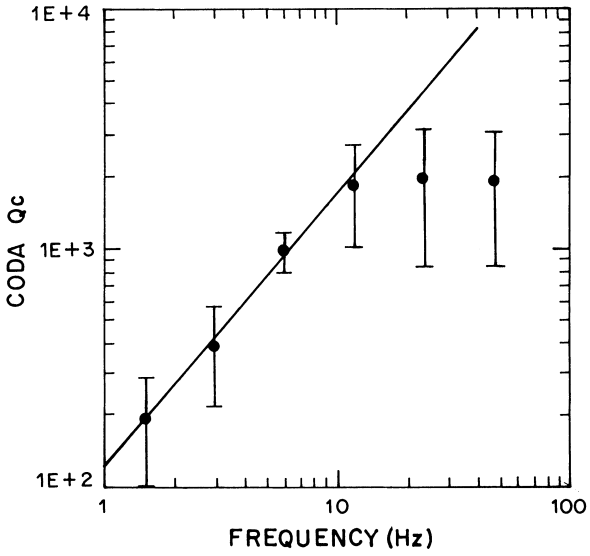

Figure 4
Fit of $Q_c = Q_0(f/f_0)^\eta$ restricted to 12 Hz, example for Region C. Q coda is determined using IASPEI software.

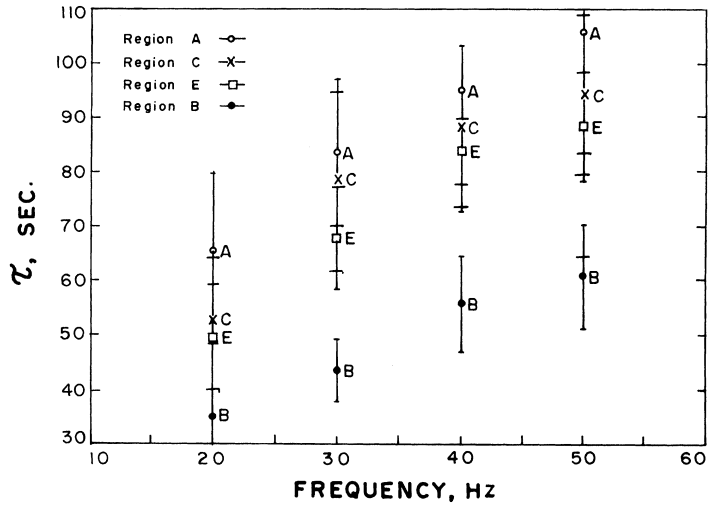

Figure 5
Fit of Q_0 as a function of coda time window τ for the different regions with the exception of D region. Due to the absence of data, X axis starts from 10 Hz and Y axis from 30 sec.

regions. The same is not true for the exponent η. This is due to the fact that there is lapse-time dependence of Q_c, while η is not lapse-time dependent. As shown in Figure 5, $Q_0(\tau)$ does not seem to follow a simple power law, although again the B region

Table 3

Least-squares fit of $Q_c(f) = Q_0 f^{\eta}$ using the values in Table 3

Region	Q_0	η
A	149 ± 55	0.9 ± 0.2
B	85 ± 32	1.3 ± 0.2
C	123 ± 31	1.1 ± 0.1
D	112 ± 60	0.9 ± 0.3
E	128 ± 60	1.1 ± 0.2

displays a different behaviour with respect to the other regions. The only exception is region D for which only four traces have passed the selection criteria, making the data almost useless. It seems that less data points give unsatisfactory results.

(b) Source Parameters

The seismic source parameters of seismic-moment, source radius and stress-drop are estimated from the *P*- and *S*-waves spectra for each earthquake. Spectral analysis is done on the FFT algorithm to get the long-period spectral level, Ω_0 and the decay γ from the displacement spectrum. Before carrying out the spectral analysis, we multiply the time series by a 20% cosine taper to retrieve the central lobe with large amplitude and reduce the rippling effect. Instrumental correction to the spectra is performed using the following relation:

$$|I(\omega)| = G \cdot \frac{(\omega^3/\omega_0^2)}{[(1-\omega^2/\omega_0)^2 + 4\,h^2(\omega^2/\omega_0)]^{1/2}}$$

Where h is the damping constant. ω_0 is the angular frequency of the free period and G is the dynamical transduction of the instrument. The velocity spectra have been corrected for the *P*- or *S*-wave attenuation and free surface effect (by dividing a factor of 2) and then transformed to diplacement, dividing by $i\,\omega$ in the frequency domain. Q-coda value is taken for the correction of spectral shape, as it is closer to the intrinsic Q_i. The error introduced in the wrong choice of Q value will give rise to the error in the estimate of long-period spectral level, Ω_0; which is much less as compared to the standard deviation of Ω_0 estimate. Consequently, the effect of Q for the attenuation correction in the spectral shape is considerably less, as compared to the large standard deviation (Table 4) in the estimate of Ω_0 value. Using the Levenberg-Marquardt algorithm (PRESS *et al.*, 1992, page 678) the observed data has been fitted to the relation given below for the Brune's seismic source model (BRUNE, 1970) in order to estimate the corner angular frequency ω_0, the long-period spectral level, Ω_0 and the decay γ from the displacement spectrum:

Table 4

Seismic source parameter estimate from P- and S-waves spectra

Sl No.	*P*-wave spectral data							*S*-wave spectral data						
	Ω_0	σ	f_0 (Hz)	σ	M_0 dyne-cm	r (km)	$\Delta\sigma$ (bar)	Ω_0	σ	f_0 (Hz)	σ	M_0 dyne-cm	r (km)	$\Delta\sigma$ (bar)
01	0.003	0.001	10.7	2.8	$0.37 \cdot 10^{21}$	0.22	159.0	0.008	0.002	9.3	1.9	$0.18 \cdot 10^{22}$	0.14	345.0
02	0.007	0.002	15.5	3.1	$0.48 \cdot 10^{21}$	0.15	707.0	0.011	0.004	11.0	3.6	$0.22 \cdot 10^{21}$	0.12	589.0
03	0.03	0.009	2.6	0.4	$0.15 \cdot 10^{24}$	0.89	108.0	0.03	0.009	5.3	0.8	$0.12 \cdot 10^{23}$	0.23	396.0
04	0.014	0.003	5.6	2.7	$0.90 \cdot 10^{23}$	0.54	449.0	0.060	0.002	3.2	0.1	$0.74 \cdot 10^{23}$	0.38	575.0
05	0.01	0.002	9.2	4.9	$0.35 \cdot 10^{23}$	0.40	565.0	0.008	0.002	7.9	3.5	$0.43 \cdot 10^{21}$	0.22	349.0
06	0.014	0.004	7.0	2.5	$0.45 \cdot 10^{23}$	0.36	587.0	0.036	0.012	6.3	2.5	$0.26 \cdot 10^{23}$	0.22	1130.0
07	0.064	0.044	12.3	3.7	$0.79 \cdot 10^{23}$	0.20	4801.0							
08	0.008	0.006	11.0	0.9	$0.95 \cdot 10^{21}$	0.20	439.0	0.016	0.007	8.0	2.5	$0.43 \cdot 10^{21}$	0.16	429.0
09	0.084	0.059	2.8	2.4	$0.23 \cdot 10^{24}$	1.21	146.0	0.031	0.009	3.2	2.3	$0.11 \cdot 10^{23}$	0.51	51.0
10								0.144	0.007	1.3	0.1	$0.15 \cdot 10^{24}$	0.92	85.0
11	0.007	0.007	13.2	2.3	$0.37 \cdot 10^{21}$	0.17	420.0	0.073	0.071	10.0	4.3	$0.52 \cdot 10^{21}$	0.14	1071.0
12	0.004	0.004	12.0	4.6	$0.25 \cdot 10^{21}$	0.21	112.0	0.023	0.032	9.0	2.4	$0.24 \cdot 10^{21}$	0.14	260.0
13	0.028	0.023	6.8	0.4	$0.74 \cdot 10^{23}$	0.33	985.0	0.028	0.014	5.9	2.0	$0.20 \cdot 10^{23}$	0.22	
14	0.005	0.002	13.1	1.8	$0.38 \cdot 10^{21}$	0.17	293.0	0.016	0.006	8.8	3.2	$0.34 \cdot 10^{21}$	0.16	
15	0.004	0.002	9.1	2.3	$0.66 \cdot 10^{21}$	0.26	166.0	0.009	0.001	7.8	0.1	$0.21 \cdot 10^{21}$	0.16	235.0
16	0.015	0.008	6.0	1.8	$0.47 \cdot 10^{23}$	0.41	389.0	0.038	0.01	5.6	0.0	$0.22 \cdot 10^{23}$	0.22	838.0
17	0.021	0.022	3.7	4.3	$0.71 \cdot 10^{23}$	1.19	43.0	0.043	0.043	2.8	0.7	$0.96 \cdot 10^{21}$	0.45	46.0
18	0.009	0.004	11.4	3.2	$0.69 \cdot 10^{21}$	0.21	348.0	0.124	0.095	8.4	3.4	$0.26 \cdot 10^{23}$	0.17	1766.0
19	0.021	0.015	9.5	6.5	$0.24 \cdot 10^{23}$	0.31	513.0	0.041	0.029	5.8	3.0	$0.12 \cdot 10^{23}$	0.26	238.0
20	0.037	0.021	7.7	4.4	$0.22 \cdot 10^{23}$	0.40	284.0	0.091	0.093	8.1	2.3	$0.51 \cdot 10^{21}$	0.16	706.0
21	0.011	0.008	1.7	0.4	$0.89 \cdot 10^{23}$	1.38	13.0	0.023	0.021	1.6	0.1	$0.30 \cdot 10^{23}$	0.78	29.0
22	0.004	0.001	8.6	9.4	$0.11 \cdot 10^{23}$	0.65	57.0	0.054	0.08	8.3	3.1	$0.26 \cdot 10^{21}$	0.18	183.0
23	0.038	0.012	6.9	2.4	$0.17 \cdot 10^{24}$	0.40	1607.0							
24	0.013	0.006	7.6	1.8	$0.21 \cdot 10^{23}$	0.30	283.0	0.053	0.006	5.2	1.6	$0.21 \cdot 10^{23}$	0.25	610.0
25	0.037	0.03	6.9	0.9	$0.64 \cdot 10^{23}$	0.33	723.0	0.139	0.061	5.1	1.1	$0.45 \cdot 10^{23}$	0.25	1269.0
26								0.006	0.001	2.6	0.1	$0.77 \cdot 10^{21}$	0.48	31.0
27	0.619	0.307	2.2	0.4	$0.34 \cdot 10^{25}$	1.01	1418.0							
28	0.038	0.032	7.5	3.4	$0.19 \cdot 10^{24}$	0.42	1063.0							

Table 4

Continued

Sl No.	*P*-wave spectral data							*S*-wave spectral data						
	Ω_0	σ	f_0 (Hz)	σ	M_0 dyne-cm	r (km)	$\Delta\sigma$ (bar)	Ω_0	σ	f_0 (Hz)	σ	M_0 dyne-cm	r (km)	$\Delta\sigma$ (bar)
29	0.019	0.013	5.0	3.9	$0.12 \cdot 10^{24}$	0.70	180.0							
30	0.008	0.005	12.6	1.5	$0.71 \cdot 10^{21}$	0.18	493.0							
31	0.021	0.033	15.7	2.5	$0.34 \cdot 10^{21}$	0.15	398.0	0.041	0.022	12.5	1.1	$0.27 \cdot 10^{21}$	0.10	1328.0
32	0.007	0.001	9.1	1.0	$0.12 \cdot 10^{23}$	0.25	377.0							
34	0.008	0.003	10.4	1.5	$0.16 \cdot 10^{23}$	0.22	602.0							
35	0.004	0.005	5.8	2.4	$0.55 \cdot 10^{21}$	0.44	39.0							
36	0.04	0.022	13.0	1.7	$0.17 \cdot 10^{23}$	0.17	1345.0							
37	0.047	0.029	5.4	2.3	$0.11 \cdot 10^{24}$	0.46	540.0	0.187	0.189	2.9	0.9	$0.15 \cdot 10^{24}$	0.46	1092.0
38	0.001	0.001	7.6	6.3	$0.15 \cdot 10^{21}$	0.45	48.0	0.933	0.027	1.3	0.1	$0.83 \cdot 10^{24}$	0.93	451.0
39	0.016	0.013	11.5	2.3	$0.32 \cdot 10^{21}$	0.20	167.0	0.735	0.416	3.0	2.6	$0.37 \cdot 10^{24}$	0.66	441.0
40	0.004	0.002	10.3	4.4	$0.10 \cdot 10^{23}$	0.26	211.0	0.928	0.033	1.3	0.1	$0.17 \cdot 10^{25}$	0.93	937.0
41	0.006	0.004	12.4	0.9	$0.56 \cdot 10^{21}$	0.18	453.0	0.927	0.035	1.3	0.1	$0.11 \cdot 10^{25}$	0.93	642.0
42	0.014	0.014	11.3	5.4	$0.17 \cdot 10^{23}$	0.22	405.0							
43	0.008	0.006	9.6	1.5	$0.43 \cdot 10^{21}$	0.24	140.0	0.579	0.488	5.3	5.5	$0.61 \cdot 10^{24}$	0.60	493.0
44	0.001	0.001	16.8	1.8	$0.43 \cdot 10^{21}$	0.13	75.0	0.022	0.013	8.3	3.1	$0.40 \cdot 10^{21}$	0.16	319.0
45	0.004	0.003	10.9	5.4	$0.57 \cdot 10^{21}$	0.28	166.0	0.938	0.02	1.3	0.1	$0.14 \cdot 10^{25}$	0.93	797.0
46	0.004	0.002	13.0	3.8	$0.35 \cdot 10^{21}$	0.19	257.0	0.919	0.039	1.3	0.1	$0.12 \cdot 10^{25}$	0.93	702.0
47	0.012	0.012	10.3	2.4	$0.26 \cdot 10^{21}$	0.23	97.0	0.809	0.309	1.9	1.4	$0.41 \cdot 10^{24}$	0.83	245.0
48	0.007	0.008	9.8	2.8	$0.19 \cdot 10^{23}$	0.26	263.0	0.62	0.425	3.1	2.7	$0.11 \cdot 10^{25}$	0.67	1055.0
49	0.009	0.008	10.3	4.6	$0.78 \cdot 10^{21}$	0.28	162.0	0.818	0.308	2.4	3.0	$0.98 \cdot 10^{24}$	0.83	634.0
50	0.032	0.013	10.5	4.7	$0.55 \cdot 10^{21}$	0.24	162.0	0.577	0.487	4.9	4.9	$0.21 \cdot 10^{24}$	0.61	212.0
51	0.014	0.012	12.0	5.1	$0.42 \cdot 10^{21}$	0.21	269.0	0.664	0.483	5.5	7.2	$0.53 \cdot 10^{24}$	0.65	687.0
53	0.047	0.021	7.0	3.5	$0.14 \cdot 10^{24}$	0.40	1135.0							
54	0.008	0.002	12.4	9.9	$0.44 \cdot 10^{21}$	0.27	388.0	0.055	0.038	13.4	5.1	$0.33 \cdot 10^{21}$	0.10	1153.0
55	0.003	0.003	3.0	0.5	$0.46 \cdot 10^{21}$	0.76	5.0	0.006	0.002	12.8	6.4	$0.28 \cdot 10^{21}$	0.11	197.0
56	0.007	0.001	12.2	2.3	$0.23 \cdot 10^{21}$	0.19	175.0							

$$\Omega(\omega) = \frac{\Omega_0}{1 + (\omega/\omega_0)^{\gamma}}.$$

Figure 6 shows examples of fit for both *P* and *S* waves. Due to the site amplification factor, some seismic stations produce larger amplitude value and the estimate of long-period spectral level, Ω_0 may be biased. The reference value is selected as the minimum Ω_0 value at a seismic station among the estimated Ω_0 values of all seismic stations for each earthquake. Due to this reason, we have not considered the long-period spectral level, Ω_0 value for the seismic station, which shows large compared to the reference

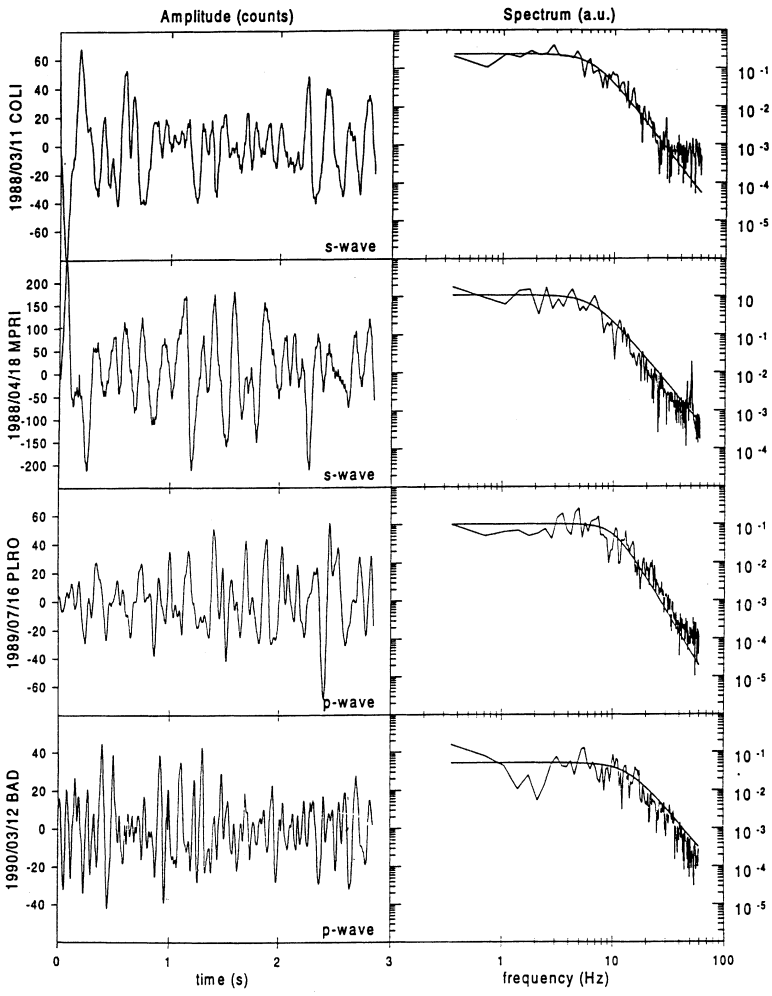

Figure 6
Seismic signal of *P* and *S* waves for a few earthquakes is shown. The amplitude spectrum of the *P* and *S* waves along with the nonlinear fit of the observed spectrum data are shown.

value by a factor of 2 or more. In this way, the stable value (± 50 percent change) of the long-period spectral level, Ω_0 for a particular earthquake is only considered.

Estimation of seismic-moment, M_0 source radius, r and stress-drop, $\Delta\sigma$ from Brune's seismic source model is accomplished using the following relation:

$$M_0 = \frac{4\pi\rho v^3 R\Omega_0}{FR_{\theta\phi}}$$

$$r = \frac{2.34v}{2\pi f_c}$$

$$\Delta\sigma = \frac{7}{16} \cdot \frac{M_0}{r^3},$$

where F is the free surface effect assumed equal to 2, ρ is the density is gm/cm^3, R is the distance from source to receiver in km, v is the P- or S-wave velocity and $R_{\theta\phi}$ is the radiation pattern correction. We use 0.6, the RMS value. All the seismic source parameter values for both P and S waves are listed in Table 4.

Results and Discussion

Coda Wave Attenuation

Region E contains all stations and enough events to determine an overall Q_c value for the region. The coda attenuation, Q_c is approximately equal to the intrinsic attenuation, Q_i (SATO and FELLER, 1998). Actually, coda at time t is mainly composed of waves backscattered by inhomogeneities in a volume shell at a distance of order $(vt)/2$ from the path connecting source and receiver. As such the coda value obtained for a region will be affected by the inhomogeneity structure of the nearby regions. In this sense the coda Q_c analysis can have a very limited spatial resolution. At a certain extent it can be controlled by limiting the length of the time window on which the coda regression is performed. In this situation the measure of the attenuation from events located in regions A, B, C and D will have commonality with scattering media of region E, of which the coda attenuation has been measured independently. Therefore the differences in the attenuation values measured in each of the surrounding regions can be interpreted as a difference in the inhomogeneity structure of that region with respect to E region.

The analysis of coda wave data for the local earthquakes in northeast Italy and its nearby regions yielded strong lateral variations of coda Q_c. The coda Q_c value is around 150–200 at the frequency of 1.5 Hz. Regions A and C show coda Q_c value of 200, while regions B, D and E show a Q_c value of 150 at the frequency of 1.5 Hz. Region D indicates a lower value of coda Q_c (304–1082) at the frequency range of 3–24 Hz, whereas regions A, B, C and E display higher values (338–1994). The coda Q_c values estimated for regions A, B, C, D and E show higher value as compared to the

estimated coda Q_c value (78 at frequency of 1.7 Hz) for the central Italy region (DEL PEZZO *et al.*, 1985; DEL PEZZO and SCARCELLA, 1986). MARGERIN *et al.* (1999) have proposed a model to interpret the coda Q_c variation in Mexico. According to MARGERIN *et al.* (1999), the coda Q_c variation can be explained by the seismic energy leakage effect due to the contrast between scattering properties of the crust and the mantle. The high coda Q_c values estimated for regions A, B, C, D and E may be due to strong variation in seismic reflectivity observed for different regions at a depth corresponding to the Moho. Above the Moho the lower crust is reflective, while below the Moho the upper mantle is generally almost transparent. The crustal reflectivity depends strongly on the geological setting (MEISSNER, 1989).

In regions A, B, C, D and E the mean free path length, l, is much larger than the crustal thickness, H; the leakage effect is small and the value of coda attenuation, Q_c is large and almost independent of the crustal thickness. In this case we expect Q_c to be mostly determined by absorption. It is suggested that the energy leakage significantly affects the coda Q_c in the low frequency range of 1.5 Hz, while at higher frequencies anelastic attenuation dominates. The presence of faults and cracks of variable sizes acts as the scatterers which are responsible for the multiple-scattering effect in northeast Italy and its vicinity (regions A, B, C, D and E). The crust beneath the region is heterogeneous which allows the scattering effect, and below the Moho depth the seismic energy leakage is small. The seismic energy leakage affects coda Q_c mostly in the crustal part only and below the Moho it is less effective.

The high coda attenuation, Q_0 (Fig. 7) is seen in the northern part of regions A and B and the southern part of C and D regions. The lithospheric thickness decreases rapidly from normal (130 km) to less than 90 km in these regions. Similarly, the Moho depth also decreases from normal 35 km to less than 30 km. The region reveals a transition at a depth from normal 35 km to less than 30 km. It shows a transition at a depth from the lower crust to the upper mantle. There is a shallow discontinuity at depths of 35 to 45 km. The region has a *P*-wave velocity of 7.0–7.5 km/sec at a depth of 20–30 km (CARROZZO *et al.*, 1981) and this high velocity is the main source of scatterers.

In general, the high seismically active region displays low coda Q_0 and the stable shield type of structure shows high Q_0 values (HERRMANN, 1980; ROECKER *et al.*, 1982; SINGH and HERRMANN, 1983). Region E is seismically more active, than other regions. The low Q_0 value (Fig. 7) is seen in Friuli (region E) which favors the above-mentioned model. In the present study the estimated high coda Q_c values (Table 2 at frequencies greater than 12 Hz may be caused by the deeper scatterers which surface from the source located in the upper mantle, having higher velocity. Due to the northward underthrusting of the African plate beneath the Eurasian plate in northeast Italy and Yugoslavia (MCKENZIE, 1972), the high density material has been formed at the deeper depth in the upper mantle, which is the main source of the scattering effect of waves and this has given rise to high coda Q_0 values (Fig. 7) in regions A, B, C, D and E.

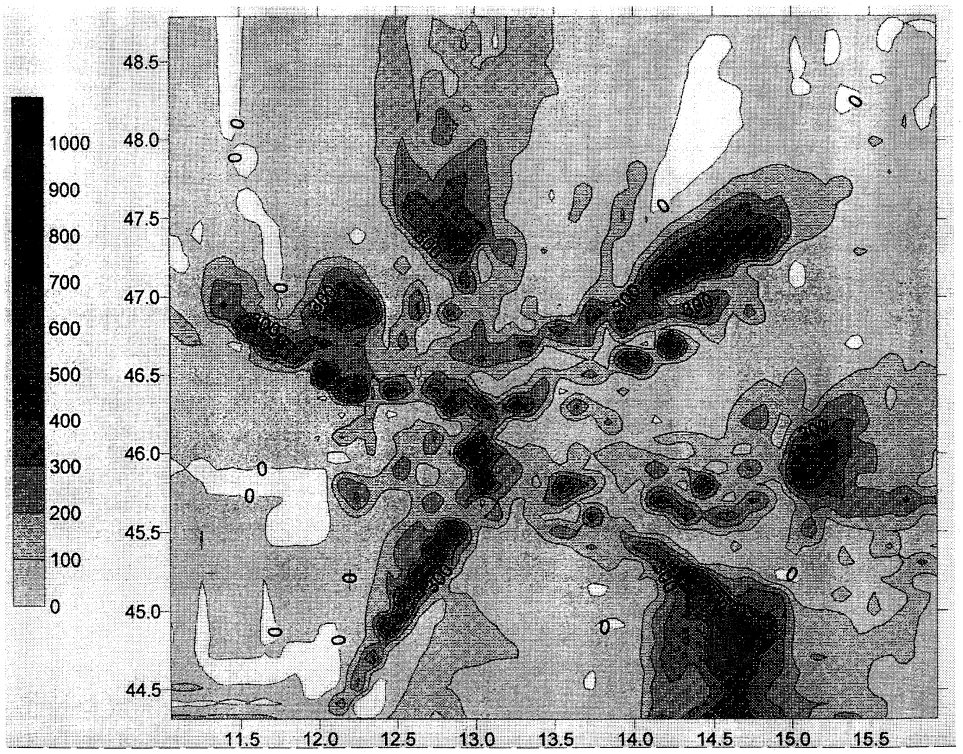

Figure 7
Two-dimensional contour map of coda Q_0 values for NE Italy and its surrounding region.

Another possible reason for higher coda attenuation, Q_c values may be due to the presence of strong scatterers close to the seismic stations in the Friuli region and/or due to the multiple scattering effect arising from the presence of well distributed heterogeneities in the entire study area (regions A, B, C, D and E). The Bouguer anomalies in the southern part of C and D regions express positive values (20 to 40 mgal), and in the northern part of B region, increase from −100 mgal to −40 mgal (SLEJKO *et al.*, 1989). The estimated lower coda Q_c value at 3–24 Hz frequency band (Table 3) of D region, compared to other regions of A, B, C and E, may be due to the high attenuating material at the deeper crustal depth in a localized zone beneath Veneto plain.

Seismic Source Parameters

Figure 8 shows the plot of seismic-moment M_0 and source radius r for both P and S waves. The source radius estimated from P wave indicates higher values compared to that of S waves and this may be due to the shift of the corner frequency

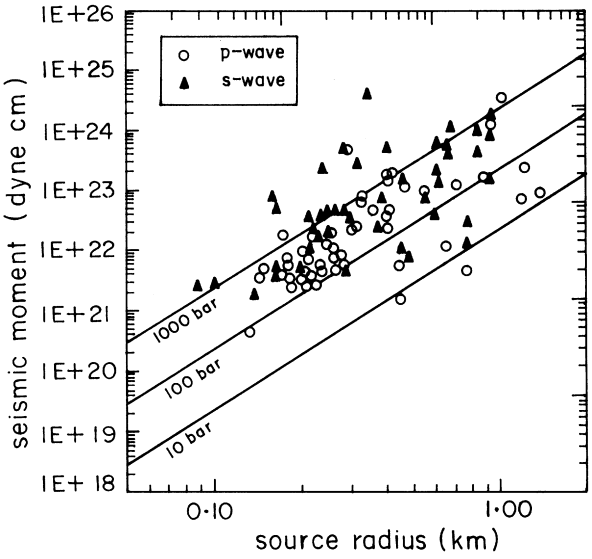

Figure 8
Plot of source radius, r versus seismic-moment, M_0 values estimated using P and S waves is plotted. The least-squares fit of the data is given in the text.

(BOATWRIGHT, 1985). The seismic moment and source radius exhibit a linear relationship (Fig. 8), and the least-squares fit between them is given as:

$$\log M_0 = (2.2 \pm 0.4) \log r + 23.3 \pm 0.3 \quad \text{for } P\text{-wave}$$
$$\log M_0 = (3.1 \pm 0.4) \log r + 24.2 \pm 0.3 \quad \text{for } S\text{-wave}$$

Figure 9 depicts the plot of seismic-moment versus stress-drop for P and S waves. In the high stress-drop region, the estimates for S waves have higher values by a maximum factor of 2 in general and also sometimes more than those for P waves, rather than in both cases a gradual increase in the stress-drop as a function of the seismic-moment in general. Although the least-squares fit between the seismic-moment and stress-drop is poor and the correlation coefficient is less than 0.5. The large scattering present in the data may result from several factors such as site amplification, significant path difference or departures from ω^2 source spectrum model (AKI, 1967). Results obtained in other studies for the Friuli region are compared in Figure 10. Our stress-drop estimates agree quite well with those obtained by NATALE *et al.* (1987) and COCCO and ROVELLI (1989). For higher stress-drop some earthquakes which have smaller seismic-moments manifest large scatter and departures from the normal values. This may derive from the reasons mentioned earlier. The Friuli earthquakes register high stress-drop values. Figure 11 shows the plot of seismic-moment versus stress-drop estimated from P and S waves for all five regions. We find a gradual increase of stress-drop with seismic moment for all

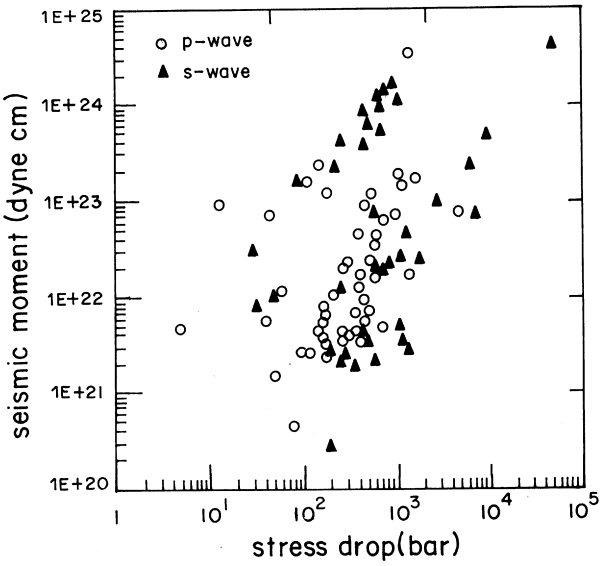

Figure 9
Plot of seismic-moment, M_0 versus stress-drop estimated using P and S waves data is shown.

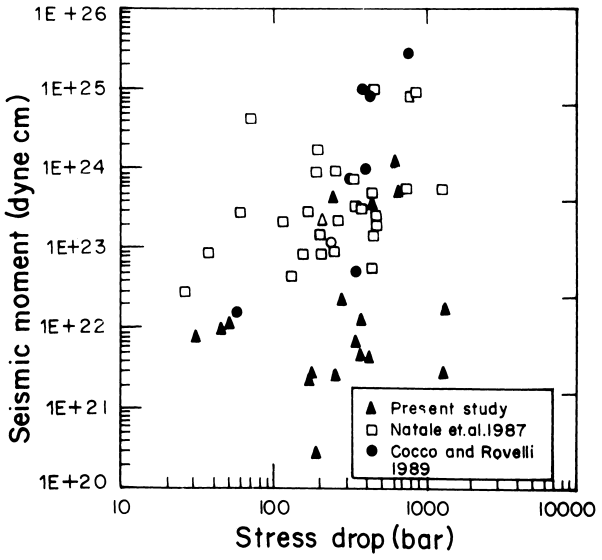

Figure 10
Plot of seismic-moment, M_0 versus stress-drop for Friuli region is shown. A comparison is made with the estimates by De Natale *et al.* (1967) and Cocco and Rovelli (1989) for the earthquakes of similar seismic-moment values.

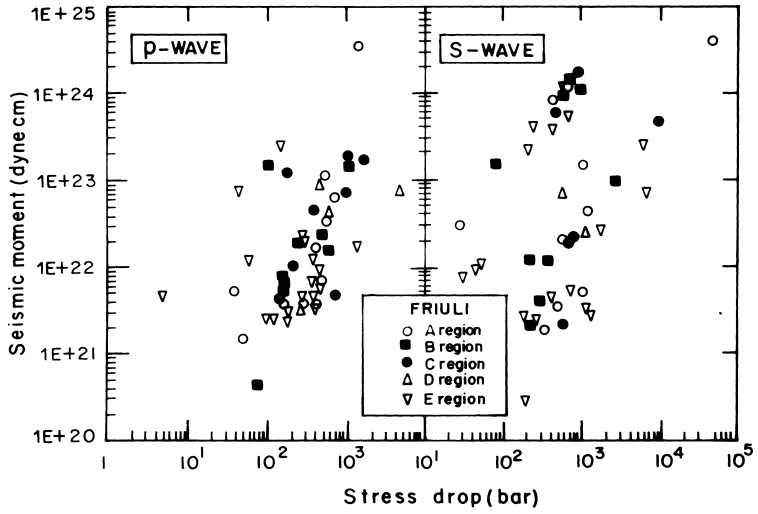

Figure 11
Plot of seismic-moment, versus stress-drop estimated using P and S waves for the five regions A to E.

regions. High stress-drop (>500 bars) earthquakes are uniformly distributed over the entire regions from A to E.

The high stress-drop earthquake causes more damage compared to the low stress-drop earthquake with the same seismic-moment/magnitude value. This results because the high stress-drop earthquake has a smaller source area (source volume) and the energy concentration is confined to a smaller source volume, i.e., it is not distributed over a wider range of source volume. As such it has a greater impact over a confined smaller region, and in the contrasting a case of low stress-drop earthquake, the same energy flux is distributed over a larger area and thereby it reduces the damage effect.

High stress-drop earthquakes originate in regions of high stress concentration which are usually generated by one or more of the following factors: (i) type of geological formations and their elastic properties, (ii) shape and size of the existing fault zone, (iii) nature of the environment, i.e., the earthquake occurred in a pre-existing fault/weak zone or it has to create a new one; (iv) the frequency of earthquake occurrence with different magnitude values.

Stress-drops of earthquakes are plotted at different focal depths in Figure 13. Due to a dense distribution of seismic stations in the Friuli region, the epicentral location of earthquakes is good with an accuracy of less than ± 2 km in the vertical and horizontal directions. We find that high stress-drop earthquakes occur at a depth of 8–14 km. This may be due to the brittle-ductile transition zone at the mid-crustal depth, where the maximum shear stress of the material is associated (CHEN and MOLNAR, 1983). A high velocity body is identified at a depth below 8 km in the Friuli

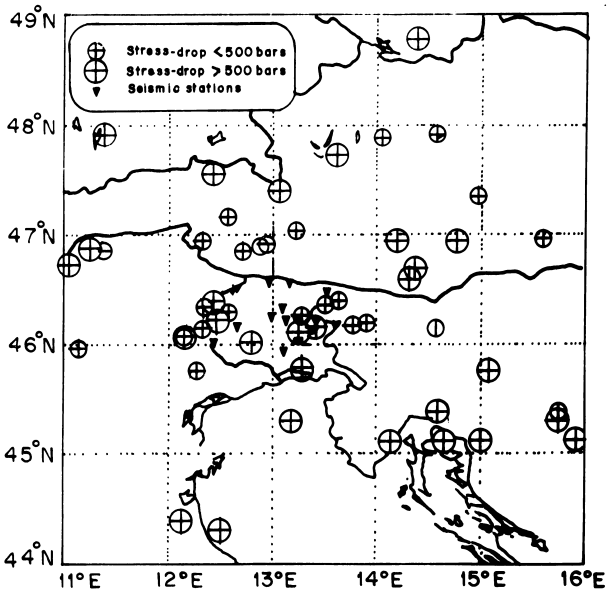

Figure 12
Plot of the epicentres of high stress-drop (> 500 bars) and low stress-drop (< 500 bars) earthquakes. The seismic stations (triangle symbol) are also shown in the figure.

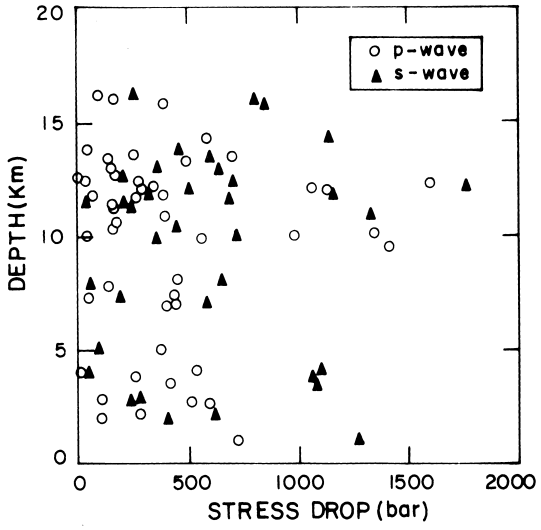

Figure 13
Plot of stress-drop of earthquakes at different focal depths estimated using *P* and *S* waves data.

region, considered as a basement, which formed due to the southward thrusted wedge of Paleozoic and matamorphic rock complex. Maximum concentration of

seismicity is observed in the depth range of 8–10 km, and below it vanishes rapidly (BRESSAN *et al.*, 1992).

Conclusions

Using a well distributed data set, a difference in the scattering properties of the zone of the NE border between Friuli and Austria has been detected. Particular attention must be devoted to the analysis of the Q_0 dependence from the time window used in the coda regression, since this parameter selects the depth at which S waves probe the scattering structure of the crust.

Results show that the scaling law relating seismic-moment to source radius $M_0 \propto r^n$ is reasonably represented by the data, giving the value of $n = 2.2$ for P wave and $n = 3.1$ for S wave; which is slightly higher compared to other global studies. The earthquakes studied in NE Italy and its surroundings have focal depths ranging from 2 to 26 km and stress-drops mainly distributed between 0.1 and 1 Kbar. A significant fraction of the events analyzed in the present study display a high stress-drop, greater than 1 Kbar, and occur at a depth of 8–14 km, indicating the presence of a brittle-ductile transition zone at mid-crustal depth.

Acknowledgments

We are grateful to Dr. Gianni Bressan for his constructive and useful discussions on the manuscript and for his guidance during the course of study. The author (D.D.S) thanks the International Centre for Theoretical Physics (ICTP), Research and Training in Italian Laboratories, Trieste for providing the funds (budget code: 5512.NLH8) for the present study and the staff members of the Osservatorio Geofisico Sperimentale, Centro Ricerche Sismologiche, Undine, Italy, who assisted and provided several facilities for completion of the research work. We extend appreciation to Dr. E. Del Pezzo of Napoli, Italy for his constructive and helpful review, which furthered our improvement of the manuscript. The author (D.D.S.) expresses gratitude to Mr. S. Thyagrajan of N.G.R.I., Hyderabad, India for his support in the preparation of the manuscript.

REFERENCES

AKI, K. (1967), *Scaling Law of Seismic Spectrum*, J. Geophys. Res. *72*, 1217–1231.

AKI, K. (1980), *Scattering and Attenuation of Shear Waves in the Lithosphere*, J. Geophys. Res. *85*, 6496–6504.

AKI, K., *Attenuation and scattering of short period seismic waves in the lithosphere*. In *Identification of Seismic Sources – Earthquake or Underground Explosion* (eds. Husebye E. S., and Mykkeltveit S.) pp. 515–541. (D. Reidel Dordrecht, Holland 1981).

AKI, K., and CHOUET, B. (1975), *Origin of Coda Waves: Sources, Attenuation and Scattering Effects*, J. Geophys. Res. *80*, 3332–3342.

AKINCI, A., TAKTAK, A. G., and REGINTAV, S. (1994), *Attenuation of Coda Waves in Western Anatolia*, Phys. Earth and Planet. Int. *87*, 155–165.

BOATWRIGHT, J. (1985), *Characteristics of Aftershock Sequence of the Borah Peak, Idaho Earthquake Determined from Digital Recordings of the Events*, Bull. Seismol. Soc. Am. *75*, 1265–1284.

BRESSAN, G., DE FRANCO, R. D., and GENTILE, G. F. (1992), *Active Faulting and Seismogenic Aspects of the Friuli Area*, Studi geologici camerti, Sp. Vol. CROP 1–1A, 89–98.

BRUNE, J. N. (1970), *Tectonic Stress and the Spectra of Seismic Waves from Earthquakes*, J. Geophys. Res. *75*, 4997–5009.

CANAS, J. A., PUJADES, L., BADAL, J., PAYO, G., MUGUEL, F., ALGUACIL, G., IBANEZ, J., and MORALES, J. (1991), *Lateral Variation and Frequency Dependence of Coda Q in the Southern Part of Iberia*, Geophys. J. Int. *107*, 57–66.

CARROZZO, M. T., LUZIO, D., EVA, C., MERLANTI, M., CALCAGNILE, G., PANZA, G., CARLI, V., CASSINIS, R., COLOMBI, B., SCARASCIA, S., MORELLI, C., PELLIS, G., COSENTINO, M., RIUSCETTI, M., NICOLICH, R., SCOTTI, A., GUERRA, I., LUONGO, G., SCARPA, R., ANSORGE, J., and MUELLER, St. (1981), *Crust and Upper Mantle Structures in the Southern Alps from Deep Seismic Sounding Profiles (1977, 1978) and Surface-wave Dispersion Analysis*, Bollett. Di Geofis. Teor. Appl. *13*, (92), 297–330.

CHEN, W. P., and Molnar, P. (1983), *Focal Depths of Intracontinental and Intraplate Earthquakes and their Implications for the Thermal and Mechanical Properties of the Lithosphere*, J. Geophys. Res. *88*, 4183–4214.

CIPAR, J. (1980), *Teleseismic Observations of the 1976 Friuli, Italy, Earthquake Sequence*, Bull. Seismol. Soc. Am. *70*, 963–983.

COCCO, M., and ROVELLI, A. (1989), *Evidence for the variation of stress drop between normal and thrust faulting earthquakes in Italy*, J. Geophys. Res. *94*, 9399–9416.

CONSOLE, R., and ROVELLI, A. (1981), *Attenuation Parameters for the Friuli Region from Strong Motion Accelerograms*, Bull. Seismol. Soc. Am. *71*, 1981–1991.

DAINTY, A. M., DUCKWORTH, R. M., and TIE, A. (1987), *Attenuation and Backscattering from Local Coda*, Bull. Seismol. Soc. Am. *77*, 1728–1747.

DE NATALE, G. D., MADARIAGA, R., SCARPAAND, R., and ZOLLO, A. (1987), *Source Parameter Analysis from Strong-motion Records of the Friuli, Italy, Earthquake Sequence (1976–1977)*, Bull. Seismol. Soc. Am. *77*, 1127–1146.

DEL PEZZO, E., ROVELLI, A., and ZONNO, G. (1985), *Seismic Q and Site Effects on Seismograms of Local Earthquakes in the Ancona Region (Central Italy)*, Annales Geophysicae *3*(5), 629–636.

DEL PEZZO, E., and SCARCELLA, G. (1986), *Three-component Coda Q in the Abruzzi-Molise Region, Central Apennines*, Ann. Geophys. *4*, 589–592.

DEL PEZZO, E., ALLOTTA, R., and PATANE, D. (1990), *Dependence of Q_c (Coda Q) on Coda Duration Time Interval; Model or Depth Effect*? Bull. Seismol. Soc. Am. *80*, 1028–1033.

FRANKEL, A., Review for '*Observational and physical basis for coda observational and physical basis for coda precursor (Jin, A. and Aki, K.)*'. In *Evaluation of Proposed Earthquake Precursors* (ed. Wyss, M.), pp. 51–53 (AGU, Washington, D.C. 1991).

HAVSKOV, J., MALONE, S., MCCLURG, D., and GROSSON, R. (1989), *Coda Q for the State of Washington*, Bull. Seismol. Soc. Am. *79*, 1024–1038.

HATZIDIMITRIOU, P. M. (1995), *S-wave Attenuation in the Crust of Northern Greece*, Bull. Seismol. Soc. Am. *85*, 1381–1387.

HERRMANN, R. B. (1980), *Q Estimates Using the Coda of Local Earthquakes*, Bull. Seismol. Soc. Am. *70*, 447–468.

IBANEZ, J. M. (1990), *Coda Wave and Lg Attenuation in South Spain and Italy Using Digital Seismograms (in Spanish)*, Ph.D. Thesis, Universidad de Granada, 306 pp.

KVAMME, L. B. and HAVSKOV, J. (1989), *Q in Southern Norway*, Bull. Seismol Soc. Am. *79*, 1575–1588.

LEE, W. H. K., AKI, K., CHOUET, B., JOHNSON, P., MARKS, S., NEWBERG, J. T., RYALL, A. S., STEWART, S. W., and TOTTINGHAM, D. M. (1986), *A Preliminary Study of Coda Q in California and Nevada*, Bull. Seismol. Am. *76*, 1143–1150.

MARGERIN, L., CAMPILLO, M., SHAPIRO, N. M., and VAN TIGGELEN, B. B. (1999), *Residence Time of Diffuse Waves in the Crust as a Physical Interpretation of Coda Q: Application to a Seismogram Recorded in Mexico*, Geophys. J. Int. *138*, 343–352.

MEISSNER, R. (1989), *Rupture, Creep, Lamellae and Crocodle Happenings in the Continental Crust*, Terra Nova *1*, 17–28.

MCKENZIE, D. P. (1972), *Active Tectonics of the Mediterranean Region*, Geophys. J. *30*, 109–185.

PHILLIPS, W. S. (1985), *The Seperation of Source, Path and Site Effects on High Frequency Seismic Waves: An Analysis Using Coda Wave Techniques*, Ph.D. Thesis M.I.T., 195 pp.

PHILLIPS, W. S., and AKI, K. (1986), *Site Amplification of Coda Waves from Local Earthquakes in Central California*, Bull. Seismol. Am. *76*, 627–648.

PRESS, W. H., TEUKOLSKY, S. A., VETTERLING, W. T., and FLANNERY, B. P., *Numerical Recipes in FORTRAN: The Art of Scientific Computing*, second edition (Cambridge University Press, 1992) 963 pp.

PUJADES, L. L., CANAS, J. A., EGOZCUE, J. J., PUIGVI, M. A., GALLART, J., LANA, X., POUS, J., and CASAS, J. (1990), *Coda Q Distribution in the Iberian Peninsula*, Geophys. J. Int. *100*, 285–302.

PULLI, J. J. (1984), *Attenuation of Coda Waves in New England*, Bull. Seismol. Sol. Am. *74*, 1149–1166.

ROECKER, S. W., TUCKER, B., KING, J., and HARTZFELD, D. (1982), *Estimates of Q in Central Asia as a Function of Frequency and Depth Using the Coda of Locally Recorded Earthquakes*, Bull. Seismol. Am. *72*, 129–149.

ROVELLI, A. (1982), *On the Frequency Dependence of Q in Friuli from Short-period Digital Records*, Bull. Seismol. Soc. Am. *72*, 2369–2372.

ROVELLI, A. (1983), *Time-frequency Analysis of Seismic Excitation of Attenuation Parameters for the Friuli (Italy) Earthquakes*, Phys. Earth Planet. Int. *33*, 94–110.

SATO, H. (1977), *Energy Propagation Including Scattering Effects, Single Isotropic Scattering Approximation*, J. Phys. Earth *25*, 27–41.

SATO, H. and FELLER, M. C., *Seismic wave propagation and scattering in the heterogeneous Earth* (Springer-Verlag, New York, Inc. 1998) 308 pp.

SINGH, S. K., and HERRMANN, R. B. (1983), *Regionalization of Crustal Coda Q in the Continental United States*, J. Geophys. Res. *88*, 527–538.

SLEJKO, D., CARULLI, G. B., NICOLICH, R., REBEZ, A., ZANFERARI, A., CAVALLIN, A., DOGLIONI, C., CARRO, F., CASTALDINI, D., ILICETO, V., SEMENZA, E., and ZANOLLA, C. (1989), *Seismotectonics of the Eastern Southern Alps: A Review*, Boll. Geof. Appl. *31*, 109–136.

VALDES, C. M., and NOVELO-CASANOVA, D. A. (1989), *User Manual for Qcoda*, Chapter 10, International Association of Seismology and Physics of the Earth's Interior, IASPEI Software Library, vol. I, 237–255.

WOODGOLD, C. R. D. (1994), *Coda Q in the Charlevoix, Quebec Region: Lapse Time Dependence and Spatial and Temporal Comparisons*, Bull. Seismol. Soc. Am. *84*, 1123–1131.

ZHUO, Y. and KANAMORI, H. (1987), *Regional Variation of the Short-period (1–10 Second) Source Spectrum*, Bull. Seismol. Am. *77*, 514–529.

(Received January 3, 2000, accepted November 20, 2000)